Pak. J. Agri. Sci., Vol. 61(3), 889-889;2024
ISSN (Print) 0552-9034, ISSN (Online) 2076-0906
DOI:10.21162/PAKJAS/24.262
http://www.pakjas.com.pk

Growth of Ag, TiO_2 and $AgTiO_2$ Nanoparticles through Liquid-Plasma Interaction for Bacterial and Wastewater Treatment

Noor ul Huda Altaf[1'*], Muhammad Yasin Naz[1*], Shazia Shukrullah[1] and Haq Nawaz Bhatti[2]

[1]Department of Physics, University of Agriculture Faisalabad, Faisalabad 38040, Pakistan; [2]Department of Chemistry, University of Agriculture Faisalabad, Faisalabad 38040, Pakistan
*Corresponding author's e-mail: noorulhuda100@yahoo.com, yasin603@yahoo.com

In this study, a one-pot liquid plasma jet technique was explored for the synthesis of silver (Ag) and titania nanoparticles (TiO_2 NPs), as well as their effective composite ($AgTiO_2$). Compared to conventional approaches, this approach involves the plasma deposition of Ag NPs onto TiO_2 NPs, which is simpler and more eco-safe. The size measurement by XRD analysis revealed the formation of Ag, TiO_2, and Ag/TiO_2 photo-catalysts with 10 nm, 15 nm, and 17 nm with UV-Vis bandgap energies of 2.58 eV, 3.36 eV, and 2.86 eV respectively. The as-synthesized catalysts were used for the degradation of Methylene blue (MB) and methyl orange (MO) dyes. Ag/TiO_2 acted as the best photo-catalyst, with 92.64 % degradation of MB and 77.5 % of MO in just 60 minutes. Integrating Ag onto TiO_2 NPs reduced the band gap with inhibited electron-hole recombination, which enhanced its reusability with minimal activity loss. Moreover, the Ag/TiO_2 photo-catalyst also showed strong antioxidant activity using the DPPH method. Integrating Ag onto TiO_2 significantly enhanced the antibacterial performance against Staphylococcus aureus and Escherichia coli. Overall findings demonstrate the potential of plasma-enhanced integration of Ag NPs onto the TiO_2 matrix for effective photocatalytic, antioxidant, and antibacterial applications.
Keywords: Wastewater, Bacteria, Silver nanoparticles, Titanium dioxide, Nonthermal Plasma, antioxidant, photo-catalysis.

INTRODUCTION

Wastewater, comprising household and industrial waste, significantly affects the environment and public health. It is estimated that 80% of the world's wastewater is discharged back into the environment without any treatment. The untreated wastewater contains numerous contaminants and toxins that can pollute water, air, and soil posing risks to ecosystem and human health (Dhamorikar *et al.*, 2024). On the other hand, notable advancements in nanomaterials have propelled global innovation in various industries in recent times. Nowadays, different NPs such as silver (Ag), gold (Au), platinum (Pt), selenium (Se), and copper (Cu) are being used for wastewater treatment. Among these, Ag NPs have attracted much attention from researchers because of their many uses, such as antibacterial (Bekmezci *et al.*, 2023), catalytic (Barani *et al.*, 2023), and sensory applications (Bose *et al.*, 2023). As such, they represent a highly promising class of materials for a wide range of industrial applications, demonstrating the rapid advancement of nanotechnology. Moreover, Ag salt and Ag-based materials are well known for their antibacterial properties since ancient times (Mustafa, 2023).

Industrial wastewater also poses a significant challenge, in addition to toxic and hazardous substances, heavy metals, and dyes that threaten the environment and human health. Many of these pollutants exhibits a stability, resistance, bathochromic shift, and color fastness to degradation, complicating their removal through conventional methods (Kashif *et al.*, 2024). Semiconductor-based photo-catalysis is the most effective, unique, and viable technique for mitigating pollutants from industrial effluents. Titanium dioxide (TiO_2) is an efficient and cost-effective photo-catalyst due to its promising properties such as, high chemical stability, high photosensitivity, excellent electronic and optical, environmental friendliness, non-toxicity, and low cost. Particularly, the anatase phase of TiO_2 is favored for its photocatalytic properties. Researchers are working to increase the photocatalytic activity of TiO_2 by doping it with transition metals like Ag, despite its snags, which include a large bandgap, high electron-hole recombination rate, short wavelength excitation, and low quantum efficiency. Ag NPs are being used to improve the effectiveness of catalytic treatment for pollutants (Ahmad *et al.*, 2024). Several studies have proven that nanomaterials' smaller size (1-100 nm) shows significant photocatalytic activity (Drdova *et al.*, 2024;

Altaf, N.H., M.Y. Naz, S. Shukrullah and H.N. Bhatti. 2024. Growth of Ag, TiO_2 and $AgTiO_2$ Nanoparticles through Liquid-Plasma Interaction for Bacterial and Wastewater Treatment. Pakistan Journal of Agricultural Sciences 61:889-889.
[Received 13 Aug 2024; Accepted 4 Sep 2024; Published 28 Sep 2024]

Halfadji *et al.*, 2024; Zeng *et al.*, 2024). Ag/TiO_2 composite is a promising candidate as photoactive material in recent research work, which strongly contributed to the optoelectronic field of visible-light-induced photocatalytic applications (Kaur *et al.*, 2023; Rahmawati *et al.*, 2023; Morante *et al.*, 2024). This modification has attracted significant attention for its potential to enhance the photocatalytic activity of TiO_2, offering a promising catalyst for wastewater treatment and environmental remediation.

However, researchers face challenges in enhancing its photocatalytic activity, such as synthesizing Ag, TiO_2, and Ag/TiO_2 NPs with controlled size, morphology, stability, and shape. Various techniques are being employed to tackle these issues, including electrochemical (Kudhier *et al.*, 2018), chemical reduction method (Duygulu *et al.*, 2024), sol-gel (Shabaninia *et al.*, 2024), sono-electrochemical (Al Baroot *et al.*, 2023), and plasma methods (Drdova *et al.*, 2024; Halfadji *et al.*, 2024; Zeng *et al.*, 2024). Among these, plasma-based methods, such as direct current glow discharge (plasma/contact non-equilibrium low-temperature plasma), have garnered great attention due to their ability to produce Ag NPs sustainably and cost-effectively (Li *et al.*, 2024). Recent studies expedite the use of capping agents in synthesis of metal NPs, with various natural and bio-organic compounds being explored for their efficacy (Altaf *et al.*, 2021a; Cyganowski *et al.*, 2023). These nanomaterials have shown exceptional photocatalytic activity, especially when degrading different contaminants when exposed to UV and visible light (Arora *et al.*, 2022; Saroha *et al.*, 2023).

Despite the promising advancements, there remains a need to systematically investigate the synthesis patterns of Ag NPs using the plasma reduction method with glucose as a stabilizer. This is significant because it can lead to the development of more efficient and cost-effective methods for producing Ag NPs. Additionally, demonstrating the efficacy of Ag NPs deposition over TiO_2 surfaces to enhance photocatalytic activity for wastewater treatment is a crucial research direction. This is important because it can contribute to the development of more effective and sustainable solutions for wastewater treatment.

Thus, this study aims to elucidate the formation patterns of Ag NPs via plasma chemical synthesis with glucose as a stabilizer and to showcase the efficiency of Ag NPs deposited over TiO_2 surfaces for improved photocatalytic activity. This study, with its potential to revolutionize the field, investigated and assessed the photocatalytic, antibacterial, and antioxidant activities of Ag NPs, TiO_2, and Ag/TiO_2 NPs, providing important insights into their synthesis and applications.

MATERIALS AND METHODS

***Materials*:** Different materials were used in the plasma reduction approach to synthesize Ag, TiO_2, and their composite NPs. The precursor for Ag NPs was silver nitrate ($AgNO_3$, ACS reagent, ≥99.0% purity), whereas the precursor for TiO_2 NPs was titanium tetrachloride ($TiCl_4$). During the synthesis process, glucose may have been used as a stabilizing agent. Deionized water was necessary for solution preparation and washing of the synthesized components, while methanol was employed as a solvent for post-treatment washing procedures. Some organic pollutants, including methylene blue (MB), and methyl orange (MO) dye, were used to evaluate the photocatalytic activity of the synthesized materials. All compounds were used just as supplied with no further purification.

***Synthesis of Ag-NPs*:** A 5 mM $AgNO_3$ and 2 mM saccharide glucose were combined to make a 100 ml solution in a traditional one-step synthesis. The impact of saccharides on Ag NPs synthesis was investigated, with parameters varied as previously detailed. After exposure to plasma, the $AgNO_3$ electrolyte separated into Ag^+ cations and NO_3^- anions ($AgNO_3^- \rightarrow Ag^+ + NO_3^-$). Active radicals and molecules, such as hydrogen peroxide (H_2O_2), hydroxyl radicals (OH), hydrogen (H), and atomic oxygen (O), were produced when plasma was ignited. These species were essential in reducing Ag^+ cations to Ag NPs ($Ag^+ + e^- \rightarrow Ag$) with hydrated electrons. Because of their high coefficient rate, irradiating electrons and H radicals from the plasma facilitated the rapid production of nanoparticles. Upon plasma exposure, the solution changed color from transparent to black over time, indicating NPs formation. Ag NPs were then separated from the solution by centrifugation and repeatedly cleaned with deionized water. The particles were then dried at 80°C in a vacuum oven for two hours.

***Synthesis of TiO_2 NPs*:** An approach that is plasma-based and similar to that utilized for producing Ag NPs is used to create TiO_2 NPs with some variations. Titanium wire is the anode electrode, and an aluminum outer electrode is the grounded electrode. The titanium anode tip is around 80 mm from the 3 mm-diameter nozzle at the bottom of the grounded electrode. $TiCl_4$ must be handled carefully with the plasma reduction process to avoid water interactions while synthesizing TiO_2 NPs. Argon (Ar) gas is delivered as a carrier at a constant flow rate of 200 (sccm) in a plasma reactor with two electrodes. $TiCl_4$ is evaporated by bubbling it with room temperature Ar gas, which allows for fine flow rate control for efficient evaporation. At a distance of 30 mm from the plasma nozzle, where the high energy plasma produced upon argon gas ionization facilitates the creation of TiO_2 NPs, the vaporized $TiCl_4$ is subsequently combined with the plasma jet effluent. Once treated, the TiO_2 NPs are collected and rinsed with deionized water to eliminate any remaining reactants. Throughout the process, safety measures are taken to reduce potential risks related to handling $TiCl_4$, such as using appropriate ventilation and personal protective equipment.

***Synthesis of $AgTiO_2$ NPs*:** The $AgTiO_2$ NPs were synthesized using a plasma reduction technique. 1 g of TiO_2 NPs were first dissolved in 100 mL of deionized water and sonicated for 30

minutes to ensure homogeneous dispersion. Subsequently, 1 % of Ag was added dropwise to the TiO_2 suspension while stirring continuously after being dissolved in 50 mL of deionized water. After that, the mixture was moved to a non-thermal plasma reactor, where an inert atmosphere was created by adding argon gas at a flow rate of 200 sccm. The discharge plasma was initiated between two electrodes, and the reactor pressure was kept at 1 atm for 30 minutes. During this time, the Ag^+ ions were reduced to metallic Ag NPs that deposited on the surface of the TiO_2. A pale-grey NPs was produced by filtering, thoroughly washing with methanol, and drying the $AgTiO_2$ NPs at 80°C for 2 hours.

***Photocatalytic Activity*:** The synthesized Ag, TiO_2, and $AgTiO_2$ NPs were used to test the photocatalytic activity for degradation of dyes, including MB and MO, under sunlight irradiation. First, a stock solution of both dyes (1000 ppm) was prepared by dissolving 100mg of MB and MO dyes in 100 ml of water. After that, a 10 ppm solution was prepared from stock solution by adding 10 ml of dye solution and 100 ml of double distilled water. After preparing 10 ppm of dye solution, the next step was adding 0.03 g of Ag NPs and 0.03 g of sodium borohydride ($NaBH_4$) as a reducing agent for a few minutes. The contaminated solution was placed under sunlight to start degrading the dye. The photocatalytic degradation of both dyes was evaluated by measuring the absorbance after 10 min intervals. The process took place by using 0.03 g of TiO_2 NPs and 0.03 g of $AgTiO_2$ catalyst with reducing agent 0.03 g of $NaBH_4$ to perform the degradation of each dye. After every 10 min, the sunlight-exposed dye solution was characterized using UV-Vis spectroscopy to check the degradation of dyes by measuring the absorbance peak. MB and MO showed maximum absorbance at 660 nm and 500 nm. The pure and composite photocatalytic activities were evaluated based on the % degradation efficiency and rate constant of the dye degradation (k) at a given time by using these equations (1,2).

$$\%\ \text{Degradation Efficiency} = \left(1 - \frac{\mathrm{A_t}}{\mathrm{A_0}}\right) \times 100 \qquad (1)$$

$$ln\frac{\mathrm{A_0}}{\mathrm{A_t}} = \mathrm{kt} \qquad (2)$$

Where, A_t is the absorbance after irradiation time t, and $A_{0,}$ is the initial absorbance.

***Reusability Test*:** The cycle experiments investigated the $AgTiO_2$ NP's stability and durability. Testing was done in three successive cycles. After each cycle, the leftover solutions from the parallel trials were mixed to recover the catalysts. After centrifugation and filtration, the recovered catalysts were cleaned with distilled water and dried at 60 °C in an oven. The next cycle experiment made use of recycled powders. The structure chemistry of recycled NPs was accomplished by FTIR analysis to perform further reusability tests.

***Assay for antimicrobial activity of against microorganisms*:** The disk diffusion method assessed the antibacterial activity of Ag NPs, TiO_2, and Ag/TiO_2 composite. Gram-positive and Gram-negative model test strains of bacteria were chosen to be Staphylococcus aureus and Escherichia coli, respectively. A confluent lawn of bacterial growth was created by evenly spreading a bacterial solution, comprising roughly 104 colony-forming units (CFUs) of recently cultivated microbial cells, on nutritional agar in Petri plates. The agar was divided into 5 mm-diameter wells using sterile borers. Then, 20 µL of Ag NPs, TiO_2, and Ag/TiO_2 composite solutions were added to each well; control wells contained only extract and water. For twenty-four hours, the plates were incubated at 37°C. The inhibition zones surrounding each sample were measured in five different directions after incubation, and the area of the inhibition zones was computed using the average values. This technique made it possible to compare different samples' antibacterial efficacy, guaranteeing precise and repeatable outcomes.

***Antioxidant activity assay*:** The DPPH Radical Scavenging Assay method assessed the antioxidant activity of obtained Ag NPs, TiO_2, and Ag/TiO_2 composites. In separate test tubes, different concentrations of prepared NPs (500, 250, 100, 50, and 10 µg/ml) and ascorbic acid were added to 1 ml DPPH solution (0.1 mM) for each assay. The mixtures were incubated for 30 mins at room temperature under dark conditions. The absorbance of the resultant solution was measured at 517 nm with ascorbic acid acting as a reference. By comparing the Ag NPs, TiO_2, and Ag/TiO_2 composite's capacities to scavenge DPPH radicals, this method allowed for the evaluation of their antioxidant potential. The DPPH free radical scavenging activity was calculated using the following equation (3).

$$\text{Scavenging Activity}\ (\%) = \frac{(\mathrm{A_0}) - (\mathrm{A_t})}{(\mathrm{A_0})} \times 100 \qquad (3)$$

Where, A_0 is the absorbance of the control solution and A_t is the absorbance of the sample.

***Characterization*:** Using an X-ray diffractometer with Cu-Kα (1.5405Å) as the radiation source, the synthesized NPs were structurally characterized. FT-IR spectroscopy on a Perkin Elmer apparatus, spanning the wavenumber range of 4000 cm^{-1} to 400 cm^{-1}, investigated surface alterations and identified functional groups. UV-visible diffuse reflectance spectroscopy (UV-2600 Shimadzu) was used to characterize and display the optical characteristics of obtained NPs. These thorough studies offer insightful information about the optical, and surface properties of the synthesized nanoparticles.

RESULTS

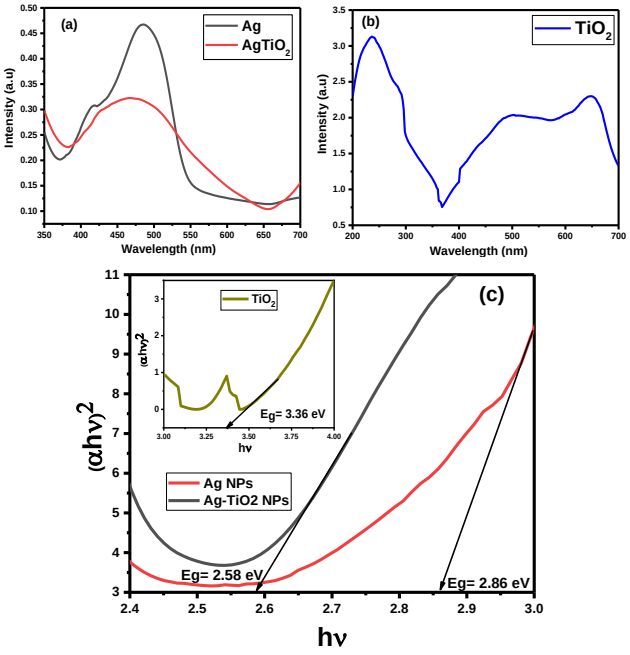

Figure 1. (a) UV-Vis absorbance spectra of glucose stabilized silver (Ag) and Ag/TiO_2 composite, (b) TiO_2 NPs, (c) Tauc plot of Silver (Ag), titania (TiO_2), and Ag/TiO_2 composite.

Table 1. Summarized Crystallite size (nm), Dislocation density (m^{-2}), Micro-strain, and Surface Area (m^2) of Silver (Ag), titania (TiO_2), and Ag/TiO_2 composite by XRD analysis.

Samples	Crystallite size (nm)	Dislocation density (m^{-2})	Micro-strain	Surface area (m^2)
Ag NPs	10	$1.00x10^{18}$	3.00×10^{-2}	$1.57x10^{-16}$
TiO_2 NPs	15	$4.44x10^{17}$	2.67×10^{-2}	$3.53x10^{-16}$
Ag/TiO_2	17	$3.53x10^{17}$	2.35×10^{-2}	$4.52x10^{-16}$

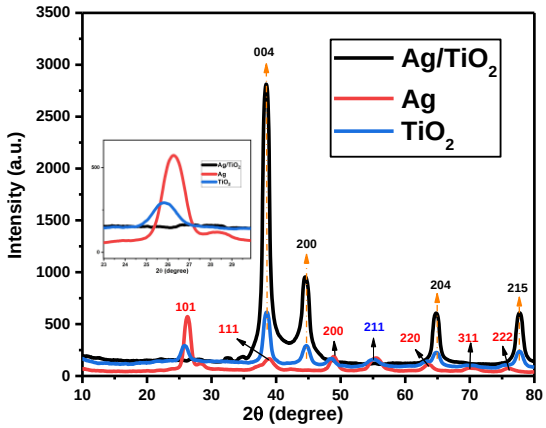

Figure 2. X-ray diffraction (XRD) patterns of silver (Ag), titania (TiO_2) and their Ag/TiO_2 composite material.

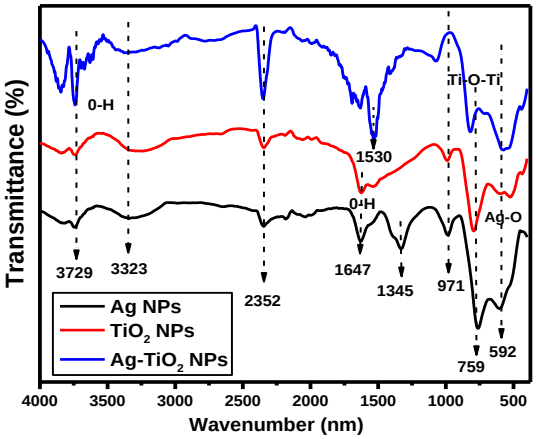

Figure 3. FTIR (Fourier-transform infrared) spectra of silver (Ag), titania (TiO_2) and their Ag/TiO_2 composite material.

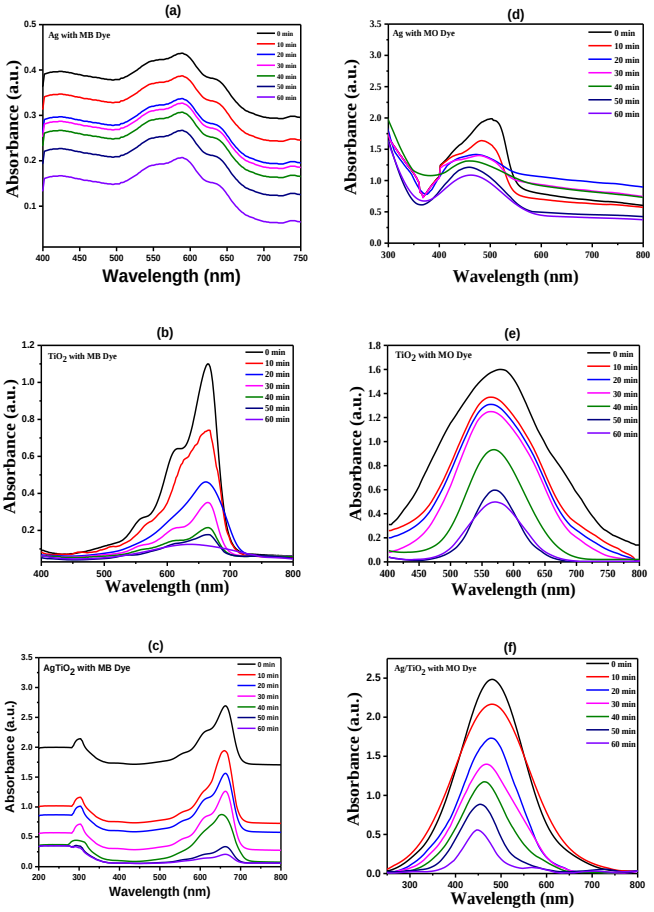

Figure 4. UV-Visible spectra revealing the degradation of methylene blue (a, b, c), and methyl orange (d, e, f) dyes using silver (Ag), titania (TiO_2) and their Ag/TiO_2 catalysts under visible light irradiation.

Table 2. Comparative % Efficiency and Kinetic Parameters for the Degradation of Methylene Blue (MB), and Methyl Orange (MO).

Photocatalysts	Efficiency (MB) (%)	Efficiency (MO) (%)	$-\ln A_t/A_0$ (MB) (min^{-1})	$-\ln A_t/A_0$ (MO) (min^{-1})	Rate Constant K_1 (MB) (s^{-1})	Rate Constant K_1 (MO) (s^{-1})
Ag	53.40	44.9	0.76547	0.59692	11.25×10^{-3}	8.88×10^{-3}
TiO_2	80.07	69.1	1.61307	1.17457	26.7×10^{-3}	19.8×10^{-3}
$AgTiO_2$	92.64	77.5	3.29584	1.49165	49.4×10^{-3}	23.7×10^{-3}

Table 3. Comparative study of influence of Reaction rate constant (k) (min^{-1}), Irradiation, Decomposing compound, and % Efficiency of Photocatalytic activity of different materials.

Photo-catalysts	Reaction rate (k) (min^{-1})	Irradiation	Degrading	% Efficiency	References
ZnO	0.0888, 0.0088	UV, Visible light	MB	90	(Wu *et al.*, 2017)
Au/Cu_2O Nanosphere	2.860	Visible light, 120 min	MB	85	(Shang *et al.*, 2013)
Ag/TiO_2	-	Visible light	gas ethylene	91.2	(Hoai *et al.*, 2023)
TiO_2 and Ag/TiO_2	0.0087, 0.0091	-	Orange G	-	(Tekin *et al.*, 2020)
NiO/Ag/TiO_2	0.03121	Visible light	MB	93.15	(Mohammed *et al.*, 2023)
Ag, TiO_2, Ag/TiO_2	0.011252, 0.0267, 0.04941	Visible light	MB	53.4, 80.07, 92.64	This study
Ag, TiO_2, Ag/TiO_2	0.0088, 0.0198, 0.0237	Visible light	MO	44.9, 69.1, 77.5	This study

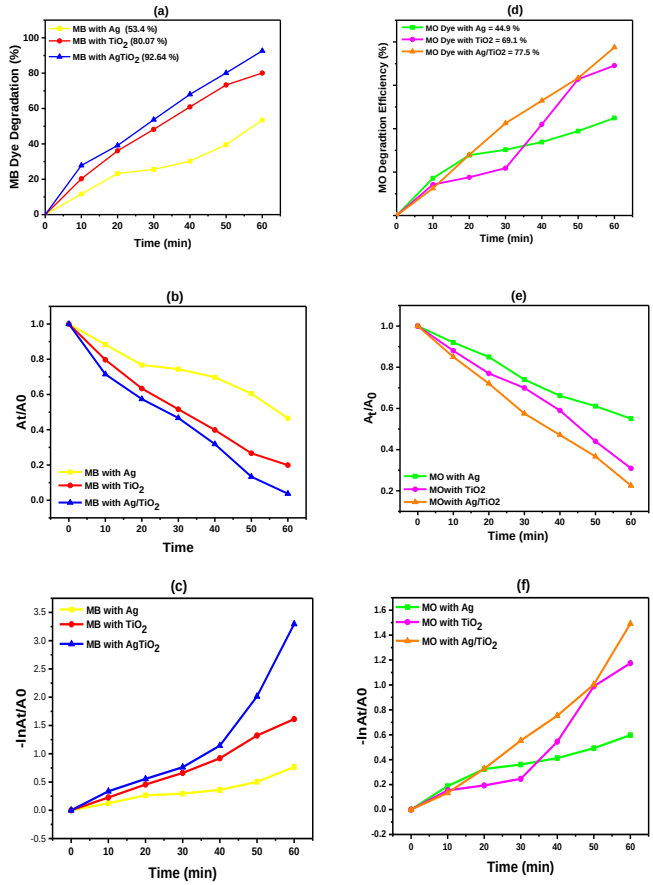

Figure 5. Kinetics graph of silver (Ag), titania (TiO_2) and their Ag/TiO_2 photo-catalysts used for the reduction of methylene blue (a, b, c), and methyl orange (d, e, f) dyes.

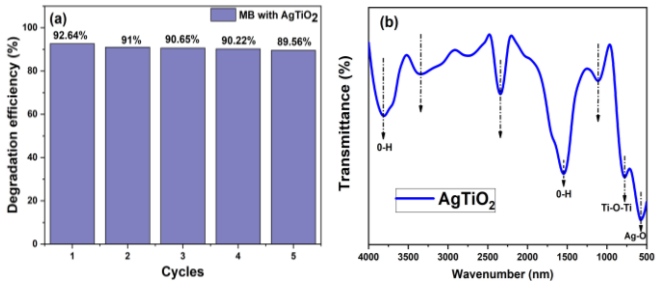

Figure 6. (a) Recycling experiments of photocatalytic degradation of dye MB over $AgTiO_2$ under visible light irradiation, (b) Fourier transform infrared spectroscopy (FTIR) spectrum of $AgTiO_2$ catalyst after photocatalytic reaction.

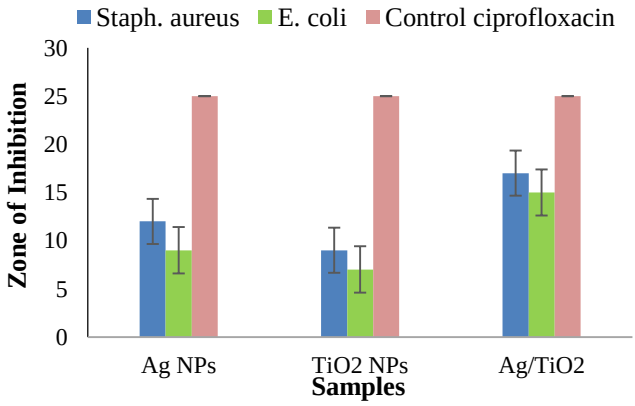

Figure 7. The inhibition zones for Gram-positive (Staphylococcus aureus) and Gram-negative (Escherichia coli) of silver (Ag), titania (TiO_2) and their Ag/TiO_2 catalyst.

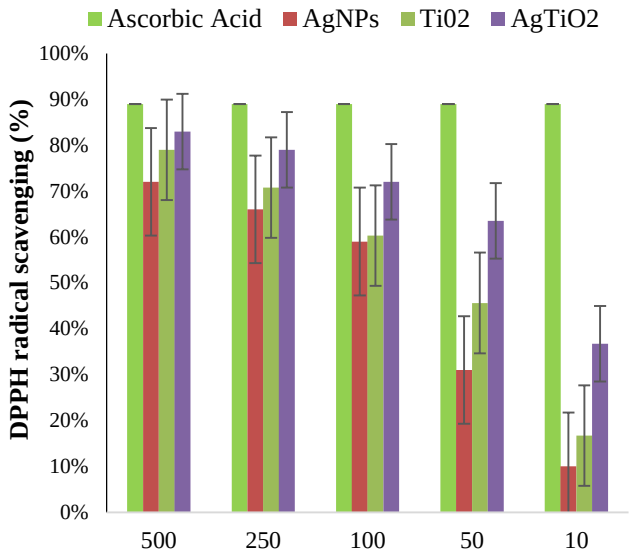

Figure 8. DPPH radical scavenging activity (%) of silver (Ag), titania (TiO_2) and their Ag/TiO_2 composite material.

DISCUSSIONS

***Optical Analysis*:** The UV-visible spectra showed a broad absorption band in the 200-700 nm range, with maximal absorption around 484 nm, which corresponds to the usual plasmon resonance band of Ag NPs as shown in Fig. 1(a) and Fig. 1(b), which confirmed the presence of Ag NPs. The size distribution, morphology, concentration, and potential aggregation of the Ag NPs all affect parameters for absorbance. Crystallite sizes and shapes are also affected by the different reagents used in the synthesis process, affecting the SPR band's position and intensity. According to UV-vis spectroscopy, the Ag solution's silvery hue abruptly became black, signifying the reduction of Ag^+ to Ag^0 and the formation of Ag NPs. This technique produces very stable Ag NPs with no discernible variation in the absorption peak's symmetry, position, or shape.

The band gap energy of pure Ag and $AgTiO_2$ catalysts corresponding to their absorption edges in UV spectra is about 2.86 eV and 2.58 eV, respectively, calculated by the Tauc plot method and shown in Fig 1(c). TiO_2 primarily absorbs UV light, as indicated by this band gap located inside the ultraviolet spectrum. The Ag/TiO_2 photocatalyst exhibited a wide absorption edge at 468 nm, extending beyond the visible light spectrum (Hamed *et al.*, 2020; Altaf *et al.*, 2021b). Pure TiO_2 has a higher band gap energy than the Ag/TiO_2 composite, which is determined to be 3.36 eV. The immobilization of Ag NPs on the TiO_2 surface is responsible for this decrease in the band gap, which causes the valence band to shift slightly higher and the conduction band to shift downward. The photocatalytic activity of the $AgTiO_2$ catalyst can be enhanced by these changes and the extension of the absorption edge into the visible range because they allow the material to absorb a wider range of sunlight. The Ag/TiO_2 composite is a more potent photocatalyst because the immobilization of Ag NPs greatly increases the visible light absorption of TiO_2.

***XRD Analysis*:** The phase composition of as-synthesized photocatalysts were studied by XRD analysis, leading to significant findings. Fig. 2 shows the XRD diffraction patterns of the as-prepared catalyst. The diffraction peaks in the XRD pattern of TiO_2 can be indexed to (101), (004), (200), 211, 204, and (215). The presence of low-intensity peaks of Ag suggests a relatively low abundance of the Ag NPs compared to TiO_2, a finding that is of great importance and has also been revealed in earlier research studies. The Scherrer Equation was employed to obtain the average crystallite size, further contributing to the significance of our findings (Ahmad *et al.*, 2024). The results indicated that the average crystallite sizes of samples, which were calcined at 100°C were 10, 15, and 17 nm. The materials' reactivity and lattice structure are greatly influenced by these tiny crystallite sizes which are in good agreement with previous studies (Duduman *et al.*, 2018). The values of the dislocation density were found to be 1 x 1018 m^{-2}, 4.44 x 1017 m^{-2}, and 3.53 x 1017 m^{-2}. Ag, TiO_2, and $AgTiO_2$ microstrain values were determined to be 3×10^{-2}, 2.67×10^{-2}, and 2.35×10^{-2}, respectively mentioned in Table 1.

***FTIR Analysis*:** FTIR analysis was used to examine the formation of oxygen functional groups onto the surface of pure Ag, TiO_2, and Ag/TiO_2 photocatalysts and their surface chemistry. Fig. 3 showing the FTIR spectra of the as-prepared catalysts. Alcohols are linked to the peak at 1345 cm^{-1}, whereas the bands at 1530 cm^{-1} and 1647 cm^{-1} are related to the acid group's -OH bonding and the symmetric/asymmetric stretching of the -COO- group, respectively. The FTIR spectra of pure Ag NPs showed numerous distinctive peaks: the Ag–O stretching mode is represented by the wideband at 592 cm^{-1}. Alkenes and aromatics are indicated by out-of-plane C–H stretching and the absorption band at 971 cm^{-1}. The OH functional group is represented by the wide absorption band at 3323 cm^{-1}. In order to produce pure and biocompatible Ag NPs, these peaks represent the interactions between silver ions and the binding sites of bioactive substances in the glucose stabilizer utilized during synthesis.

The TiO_2 lattice vibration, also known as the Ti–O stretching mode, is responsible for the noticeable absorption band that was observed in the TiO_2 catalyst's FTIR spectrum at 759 cm^{-1}. The hydroxyl groups' O–H stretching is also represented by the peaks at 3729 cm^{-1}. The broad band between 2900 and 3420 cm^{-1} is linked to water adsorbed onto the surface of the NPs and their H–O–H bending vibrations (Shabaninia *et al.*, 2024). As scavengers of photogenerated electrons and holes, these hydroxyl groups are essential for increasing photocatalytic activity because they produce hydroxyl

radicals (OH), which are vital for the removal of contaminants. Ag and TiO_2 bands were combined in the Ag/TiO_2 catalyst's FTIR spectra. The stretching and bending vibrations of the Ti-O-Ti bond in $AgTiO_2$ are represented by the Ag–O stretching mode at 592 cm^{-1}, the Ti–O stretching modes at 759 cm^{-1} and 3729 cm^{-1} for O–H stretching vibrations located in this relevant range (2900 - 3420 cm^{-1}) (Sukhadeve *et al.*, 2023). Other transmittance peaks confirmed interactions of Ag NPs with TiO_2 noticed at 500–750 cm^{-1}, which is caused by OH vibrations from H–OH – H interactions and hydrogen bonding among Ag NPs and TiO_2 NPs. The role of the present functional groups and interactions of these groups significantly contributed to the photocatalytic properties of Ag/TiO_2 nanocomposites. Overall, FTIR analysis indicates the existence of functional groups, and their interaction significantly contributes to increasing the photocatalytic activity and stability of corresponding NPs.

***Catalytic reduction of MB and MO over Ag/TiO_2 nanocomposite*:** Following the comprehensive characterization of the synthesized NPs, their catalytic efficacy was evaluated by reducing two organic dyes (MB and MO) in water-contaminated samples in the presence of sodium borohydride ($NaBH_4$) as a reducing agent. The reaction progress was continuously monitored using a UV-Vis spectrophotometer, and the resulting absorbance spectra are depicted in Fig. 4. Before adding $NaBH_4$ and catalyst, the dilute aqueous dye solution exhibited a distinctive color. Upon commencement of the reaction, the solution's color swiftly began to fade, signaling the degradation process. This alteration in color correlates with shifts in absorption frequencies (λmax) detected by the UV-Vis spectrophotometer.

The photocatalytic degradation of dyes such as MB and MO using Ag, TiO_2 NPs, and Ag/TiO_2 composite was discussed below. When light falls on metal NPs such as TiO_2 and Ag, the electrons move from the valance band to the conduction band. The electron-hole pairs move separately on the surface of NPs, and these help to perform the oxidation/reduction reaction with water and oxygen, producing reactive species. These reactive species react with dyes to degrade them. In the presence of a reducing agent, the removal of dyes was less efficient, but after adding metal NPs, the maximum and efficient degradation of dyes was achieved. The reducing agent was to create reactive species or radicals that help in the degradation process. The result showed that maximum dye degradation is only possible in the presence of metal NPs and reducing agents. In the case of Ag catalyst, MB and MO degradation was observed to be 53.4% and 44.9% respectively. Similarly, the dye degradation efficiency using TiO_2 catalyst was observed to be 80.07 %, and 69.1 % whereas, the degradation efficiency of both dyes in the presence of Ag/TiO_2 catalyst was observed to be 92.64 % and 77.5 % respectively showed in Fig. 4 (a, b, c) for MB dye and Fig. 4 (d, e, f) for MO dye.

TiO_2 and Ag catalysts do not show a significant photocatalytic efficiency in sunlight compared to $AgTiO_2$. The reason is that due to the wide band gap of TiO_2, it can be activated under UV light only, which is 5 % of sunlight. In contrast, Ag/TiO_2 has a narrow band gap, so it can be activated easily under visible light, which is important in increasing the lifetime of photo-generated electron-hole pairs. These photo-generated electron-hole pairs are responsible for an oxidation/reduction reaction with species absorbed on the surface of NPs to generate reactive species, which, as a result, react with dyes and reduce agents to achieve efficient degradation. The doping ratio also plays an important role in photocatalytic reactions. Only 1 % of Ag NPs doped TiO_2 NPs showed higher photocatalytic activity towards both dyes, such as MB and MO.

Another important factor that affects the photocatalytic activity of Ag, TiO_2, and $AgTiO_2$ NPs is the pH of the solution. Thus, the photocatalytic efficiency of Ag, TiO_2, and $AgTiO_2$ NPs was tested at different starting pH of the solution (3, 5, 7, and 9) at different intervals while maintaining a fixed catalyst dosage of 10 mg and dye concentration of 10 ppm. The results illustrated in Fig. 5. show that Ag-doped TiO_2 NPs have higher photocatalytic activity in an alkaline medium (pH greater than 7) than in an acidic medium. It happens because TiO_2 NPs tend to undergo photo-dissolution in acidic media (pH of 3). Thus, in photo-catalysis alkaline medium often enhances the reaction mechanisms, which is in good agreement with the results of Kuruva and his coworker's study (Kuruva *et al.*, 2024).

***The mechanistic study*:** A plausible mechanistic pathway for the reduction of MB and MO dyes using the Ag, TiO_2 and Ag/TiO_2 nanocomposite in aqueous medium is proposed, as illustrated in Fig 9, and their mechanistic pathway as follows in equations (4-10):

$$AgTiO_2 + h\upsilon \text{ (light energy)} \rightarrow AgTiO_2\ (e^- + h^+) \quad (4)$$

$$h^+ + H_2O \rightarrow *OH \quad (5)$$

$$e^- + O_2 \rightarrow *O_2^- \quad (6)$$

$$\text{Dye} + AgTiO_2 \rightarrow \text{Dye} - AgTiO_2 \text{ (adsorbed complex)} \quad (7)$$

$$*OH \text{ or } (*O_2^-) + \text{Dye} \rightarrow \text{degraded products} \quad (8)$$

$$\text{degraded products} + *OH\ (*O_2^-) \rightarrow CO_2 + H_2O \text{ mineralized products} \quad (9)$$

$$AgTiO_2(e^- + h^+) \rightarrow AgTiO_2 \text{ (regenerated)} \quad (10)$$

Initially, $NaBH_4$ dissociates to yield borohydride ions, which then adsorb onto the surface of the photo-catalyst. Simultaneously, the dye molecules are adsorbed onto the catalyst surface through π-π stacking interactions. Hydrogen ions (H^-) are subsequently transferred to the dye molecules, leading to their reduction. Eventually, the reduced dye molecules desorb from the nanocomposite surface, leaving the catalytic sites available for subsequent cycles (Narayan and Bezborah, 2024).

Even though metal oxide nanoparticles have a brief recombination lifespan, their catalytic activity is established. However, the efficiency of photocatalytic degradation is

increased when a surface plasmon resonance (SPR) metal, such silver (Ag), is added. This results in electron shrinkage and lengthens the recombination time. In order to create valence band defects (holes occupation), this work attempted to recombine excitation electrons from the valence band with conduction band holes. Ag metals attract the electrons to the conduction band, and electrons are bound in the Ag core to help in charge separation and reducing recombination (Nethravathi *et al.*, 2022).

Plasmonic metals were introduced in NP's outer shell to surpass the demerit of visible light absorption. This proves the enhancement of photocatalytic activity and dye degradation using visible light, showing NPs can remove harmful agents. Kinetic studies Fig. 5 reveal distinct behaviors and mechanisms for Ag, TiO_2, and Ag/TiO_2 catalysts, illustrating the decolorization rates and degradation efficiencies. The different kinetic behaviors and reaction mechanisms of Ag, TiO_2, and Ag/TiO_2 catalysts generated by a plasma reduction approach can explain the observed decolorization rate and degradation efficiencies of MB dye (Fig. 5(a, b, c)), and MO dye (Fig. 5(d, e, f)). Similar to the photocatalytic efficiency, the pseudo-first-order values and the rate constants K_1 demonstrate that Ag/TiO_2 nanocomposites have the greatest values, followed by TiO_2 NPs and Ag NPs. Faster dye degradation is indicated by higher pseudo-first-order and K_1 values, which is in line with the reported efficiencies. Ag and TiO_2 combine synergistically in the nanocomposite to provide improved photocatalytic performance, as seen by the significant rise in the rate constants for Ag/TiO_2 when compared to TiO_2 alone. The efficiency and reaction kinetics of different samples for the two pollutants MB (methylene blue) and MO (methyl orange) are summarized in Table 2.

This improvement is more noticeable for MB than MO, indicating that the Ag/TiO_2 composite has a greater affinity or reactivity for MB in the experimental setup. The increased surface characteristics and synergistic effects of the plasma reduction approach lead to more effective catalytic activity for dye degradation, as seen by the improved performance of Ag/TiO_2 in the pseudo- first -order model.

Terpenoids and hydroxyl groups play vital roles in photocatalytic dye degradation by enhanced reducing recombination, expanding the photocatalyst's light absorption spectrum, charge separation, preserving photocatalyst activity, and scavenging reactive oxygen species. Hydroxyl groups produce reactive hydroxyl radicals, improving surface hydrophilicity and dye adsorption. Terpenoids and hydroxyl groups collectively enhance surface contacts, ROS production, and photocatalytic dye degradation. Fig.9 illustrates the photocatalytic degradation mechanism of Ag/TiO_2 photocatalysts. The reduction of MB and MO dyes is reported in Table 3. to highlight the benefits of this method over previous research. These findings demonstrate the catalysts' effectiveness compared to previously reported catalysts, especially regarding the rate constants.

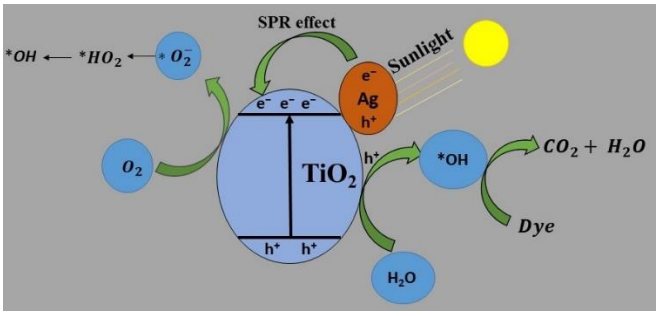

Figure 9. Schematic diagram of photo-catalysis reaction mechanism silver doped titania (Ag/TiO_2) under visible light irradiation.

***Recycle-ability and stability Test*:** A catalyst's capacity for reuse is one of its most important characteristics. Five successive cycles of the $AgTiO_2$ catalyst's recyclability test were examined. After the first cycle, the nano-catalyst was recovered by centrifugation and then cleaned three times with DI water and then again with ethanol. It was cleaned, dried in an oven for 12 hours at 80 °C, and then returned to use. Five cycles involved catalysts' recovery, cleaning, drying, and reuse. Fig. 6 (a) illustrates the proportion of MB dye that mineralized throughout each run and shows that the performance of the nano-catalyst decreased slightly following each recycling procedure. This slight decrease in catalyst activity can be attributed to catalyst loss throughout the recycling process.

***Stability Test*:** Moreover, the $AgTiO_2$ catalyst that had been recovered after the fifth cycle was thoroughly analyzed using FTIR to confirm stability and obtain insight into the surface chemistry of recycled particles. Fig. 6(b) clearly shows no discernible change in the FTIR and no noteworthy alteration in peak absorbance during the reuse cycles. Peak intensity variations or the elimination of peaks connected to active sites (Ag-O, Ti-O, etc.) may be signs that these sites are being blocked or modified, which would lower catalytic effectiveness.

The FTIR spectrum obtained from reusability testing is crucial to assess the Ag/TiO_2 catalyst's long-term vitality. By comparing the spectra of the catalyst before Fig. 3 and after reuse Fig. 6 (b), one may ascertain whether it maintains its structural integrity and functional groups, pinpoint the causes of any activity loss, and validate the catalyst's suitability for recurrent usage. These findings demonstrated that the $AgTiO_2$ catalysts generated by plasma were extremely stable and could be used again to decompose organic contaminants successfully (Aoudjit *et al.*, 2021).

***Antibacterial Activity*:** The antibacterial activity of the as-prepared Ag, TiO_2, and Ag/TiO_2 catalysts has been extensively studied. These nanoparticles are tested against Gram-positive (Staphylococcus aureus) and Gram-negative (Escherichia coli) bacteria to determine their antibacterial efficacy. In particular, the Ag–TiO_2 catalyst effectively

inhibits the growth of microorganisms. Comparative tests against pure TiO_2, a control antibiotic (ciprofloxacin), and pure Ag showed that Ag–TiO_2 catalysts have superior antibacterial capabilities.

The antibacterial activity of TiO_2 was greatly enhanced by adding Ag, which expanded the inhibition zones for S. aureus and E. coli from 9 mm to 17 mm and 7 mm to 15 mm, respectively, as demonstrated in Fig. 7. The results suggest that the $AgTiO_2$ catalyst has better antibacterial capabilities, even though the control drug, ciprofloxacin, showed a substantially higher inhibition. However, Ag^+ released from the composite material destroys the bacterial cell wall and harms the bacteria, producing an antibacterial action. Concurrently, the dispersibility, bioavailability, and stability of nanoparticles are enhanced by the presence of bio-active chemicals, hence augmenting their antimicrobial characteristics (Hidayat *et al.*, 2024). The observed results of this study, in conjunction with those of a prior study, show that doping Ag NPs and TiO_2 surfaces with metal or metal oxide increases the electrons and holes charge separation by lowering the band gap energy, hindering recombination rate, and enhancing antibacterial activity. Thus, in our present study, the presence of Ag in TiO_2 significantly enhanced the antibacterial properties of TiO_2 (Ali *et al.*, 2018; Kudhier *et al.*, 2018).

***Antioxidant Activity*:** The antioxidant properties of silver (Ag), titanium dioxide (TiO_2), and a composite of Ag and TiO_2 were evaluated using the DPPH free radical scavenging assay. The results showed that the antioxidant activity of the materials increased as their concentrations rose. However, ascorbic acid, a well-known antioxidant, demonstrated higher activity than the prepared materials at all concentrations. The Ag/TiO_2 composite exhibited exceptional antioxidant activity, inhibiting the DPPH radical effectively. These findings are consistent with previous studies on the antioxidant properties of nanomaterials, suggesting potential applications for the Ag/TiO_2 composite in various fields (Nasseri *et al.*, 2020; Alhar *et al.*, 2023). DPPH radical scavenging activity of pure and Ag/TiO_2 is presented in Fig. 8. The antioxidant activity of $AgTiO_2$ was higher than pure Ag and TiO_2 at each concentration when the pure and $AgTiO_2$ catalyst concentrations rose from 10-500 µg/ml. The maximum antioxidant activities of Ag NPs, TiO_2, and Ag/TiO_2 catalysts were 72%, 79%, and 83%, respectively, for 500 µg/ml concentration—the highest radical inhibition ability achieved with $AgTiO_2$ catalyst as 83%. Therefore, the results show that the antioxidant activity of metal and metal oxide materials is dose-dependent. A few studies have focused on the antioxidant activity of pure and metal oxide materials concerning the structure, shape, size, and concentration of the material. For example, Eskikaya and his coworkers investigated the antioxidant activity of ZnO–NF_2, which was found to be higher than ZnO–NF_1 at each concentration (82.32% and 87.18% for ZnO–NF_1 and ZnO–NF_2, respectively, at 200 mg/mL) (Eskikaya *et al.*, 2022). Ayodhya and Veerabhadram synthesized the g-C_3N_4/Ag_2S composite by sonochemical method and evaluated a higher % scavenging activity that depends on conc. Of materials (0.3 to 3.0 µM concentration) (Ayodhya and Veerabhadram, 2019). Guerriche and colleagues used a hydrothermal technique to successfully deposit different concentrations of silver nanoparticles (Ag NPs) on titanium dioxide (TiO_2) and evaluated their antibacterial and antioxidant properties. The Ag-TiO_2 composites effectively neutralized the DPPH radical, while pure TiO_2 and materials with low silver content (0.1, 1.5, 3%) had no discernible effect. Higher silver concentrations (5 and 10%) boosted the antioxidant activity, most likely due to the nature and quantity of Ag NPs, as reported by various authors (Boudghene-Guerriche *et al.*, 2020).

***Conclusions*:** The glucose-stabilized, plasma-enhanced synthesis of Ag/TiO_2 nanocomposite demonstrates significant improvements in photocatalytic, antioxidant, and antibacterial activities compared to pure Ag and TiO_2 NPs. The plasma reduction method, with its simplicity and environmental friendliness, NPs yields with well-defined sizes and enhanced properties. The composite's reduced band gap and inhibited electron-hole recombination contribute to its superior photocatalytic efficiency under natural sunlight, achieving high degradation rates of methylene blue (MB) and methyl orange (MO). The catalyst, after being centrifuged and dried for the next cycle, lost only 2% efficiency after completing five degradation cycles, confirming the stability and reusability of the Ag/TiO_2 nanocomposite. Additionally, the Ag/TiO_2 nanocomposite exhibits robust antioxidant activity and substantial antibacterial performance against Staphylococcus aureus and Escherichia coli.

Further research is suggested to examine the effect of plasma parameters and gas type on the structures of the nanocomposites. These factors play a crucial role in the synthesis process and their optimization could lead to further improvements in the properties of the nanocomposite. Additionally, the effect of multiple stabilizers on the production and immobilization of Ag NPs on TiO_2 NPs should be considered in future studies. These findings underscore the potential of Ag/TiO_2 as a multifunctional material for diverse environmental and biomedical applications.

***Conflict of Interest*:** The Authors declare that there is no conflict of interest.

***Authors' contributions*:** Conceptualization, analysis, and writing by NUHA, HNB; validation, whereas YN and SS conceived the idea and supervised the work. All authors have reviewed and approved the final version of the manuscript.

***Acknowledgement*:** Authors acknowledge no funding source.

REFERENCES

Ahmad, I., M.A. Aftab, A. Fatima, S.D. Mekkey, S. Melhi and S. Ikram. 2024. A comprehensive review on the advancement of transition metals incorporated on functional magnetic nanocomposites for the catalytic reduction and photocatalytic degradation of organic pollutants. Coordination Chemistry Reviews 514:215904.

Al Baroot, A., S.A. Haladu, S.M. Magami, S. Akhtar, Q. Drmosh, K.A. Elsayed and A.A. Manda. 2023. Photocatalytic performance of $Ag/TiO_2/SiO_2$ nanocomposite synthesized by eco-friendly pulsed laser ablation technique. Journal of Physics and Chemistry of Solids 180:111489.

Alhar, M.S.O., D. Muhammad, K. Tahir, M.E. Zaki, M. Urooj, S. Nazir, K. Albalawi, H.S. Al-Shehri, E.A.M. Saleh and A.U. Khan. 2023. An Eco-Benign Biomimetic Approach for the Synthesis of Ni/ZnO Nanocomposite: Photocatalytic and Antioxidant Activities. Molecules 28:1705.

Ali, T., A. Ahmed, U. Alam, I. Uddin, P. Tripathi and M. Muneer. 2018. Enhanced photocatalytic and antibacterial activities of Ag-doped TiO_2 nanoparticles under visible light. Materials Chemistry and Physics 212:325-335.

Altaf, N.U.H., M.Y. Naz, S. Shukrullah, H.N. Bhatti, M. Irfan, M.A. Alsaiari, S. Rahman, U.M. Niazi, A. Glowacz and K. Proniewska. 2021a. Statistically optimized production of saccharides stabilized silver nanoparticles using liquid–plasma reduction approach for antibacterial treatment of water. Materials 14:5841.

Altaf, N.U.H., M.Y. Naz, S. Shukrullah, A. Ghaffar, M. Irfan, D. Walczak, A. Głowacz, M.H. Mahnashi, S. Rahman and G. Królczyk. 2021b. Concurrent synthesis and immobilization of Ag nanoparticles over TiO_2 via plasma reduction for photocatalytic treatment of methyl blue in water. Materials 14:6082.

Aoudjit, L., H. Salazar, D. Zioui, A. Sebti, P.M. Martins and S. Lanceros-Mendez. 2021. Reusable Ag@ TiO_2-based photocatalytic nanocomposite membranes for solar degradation of contaminants of emerging concern. Polymers 13:3718.

Arora, I., H. Chawla, A. Chandra, S. Sagadevan and S. Garg. 2022. Advances in the strategies for enhancing the photocatalytic activity of TiO_2: Conversion from UV-light active to visible-light active photocatalyst. Inorganic Chemistry Communications 143:109700.

Ayodhya, D. and G. Veerabhadram. 2019. Synthesis and characterization of g-C_3N_4 nanosheets decorated Ag_2S composites for investigation of catalytic reduction of 4-nitrophenol, antioxidant and antimicrobial activities. Journal of Molecular Structure 1186:423-433.

Barani, A., S.R. Alizadeh and M.A. Ebrahimzadeh. 2023. A comprehensive review on catalytic activities of green-synthesized selenium nanoparticles on dye removal for wastewater treatment. Water 15:3295.

Bekmezci, M., H. Ozturk, M. Akin, R. Bayat, F. Sen, R. Darabi and H. Karimi-Maleh. 2023. Bimetallic biogenic Pt-Ag nanoparticle and their application for electrochemical dopamine sensor. Biosensors 13:531.

Bose, S., S.A. Raj, J. Srivastava, U. Kumar and A. Kapahi. 2023. Carbon nanotube based biosensor: An update. In: AIP Conference Proceedings.

Boudghene-Guerriche, A., H. Chaker, M. Aissaoui, I. Chikhi, K. Saidi-Bendahou, N. Moukhtari-Soulimane and S. Fourmentin. 2020. Evaluation of antibacterial and antioxidant activities of silver-decorated TiO_2 nanoparticles. ChemistrySelect 5:11078-11084.

Cyganowski, P., M. Caban, M.A. Khan, M.M. Marzec, A. Zak, P. Pohl, P. Jamroz, A. Bernasik and A. Dzimitrowicz. 2023. The use of cold atmospheric pressure plasma for the synthesis of saccharide-stabilized Re nanostructures enabling effective deactivation of nitro-based antimicrobial agents. Plasma Chemistry and Plasma Processing 43:199-224.

Dhamorikar, R.S., V.G. Lade, P.V. Kewalramani and A.B. Bindwal. 2024. Review on integrated advanced oxidation processes for water and wastewater treatment. Journal of Industrial and Engineering Chemistry 138:104-122

Drdova, S., M. Gao, O. Sambalova, R. Pauer, Z. Zhou, S. Dimitriadou, A. Schmidt-Ott and J. Wang. 2024. Precursor-and waste-free synthesis of spark-ablated nanoparticles with enhanced photocatalytic activity and stability towards airborne organic pollutant degradation. Environmental Science: Nano 11:1023-1043.

Duduman, C.N., M. Harja, M.I. Barrena Pérez, C.G. de Castro, D. Lutic, O. Kotova and I. Cretescu. 2018. Preparation and characterization of nanocomposite material based on tio 2-ag for environmental applications. Environmental Engineering & Management Journal (EEMJ) 17:925-936.

Duygulu, N.E., A. Altinbay and F. Ciftci. 2024. Antibacterial, Mechanical, and Thermal Properties of Ag, ZnO, TiO_2 Reinforced PVA Nanocomposite Fibers. ChemistrySelect. 9:e202402311.

Eskikaya, O., S. Ozdemir, G. Tollu, N. Dizge, R. Ramaraj, A. Manivannan and D. Balakrishnan. 2022. Synthesis of two different zinc oxide nanoflowers and comparison of antioxidant and photocatalytic activity Chemosphere. 306:135389.

Halfadji, A., M. Naous, S. Rajendrachari, Y. Ceylan, K.B. Ceylan and P.R. Shekar. 2024. Effective investigation of electro-catalytic, photocatalytic, and antimicrobial properties of porous CuO nanoparticles green synthesized using leaves of Cupressocyparis leylandii. Journal of Molecular Structure 1301:137318.

Hamed, N., M. Ahmad, N. Hairom, A. Faridah, M. Mamat, A. Mohamed, A. Suriani, N. Nafarizal, F. Fazli and S.

Mokhtar. 2020. Dependence of photocatalysis on electron trapping in Ag-doped flowerlike rutile-phase TiO_2 film by facile hydrothermal method. Applied Surface Science 534:147571.

Hidayat, R., G. Fadillah, S.I. Ohira, F.I. Fajarwati, D.A. Setyorini and A. Saputra. 2024. Facile green synthesis of Ag doped TiO_2 nanoparticles using maple leaf for bisphenol-A degradation and its antibacterial properties. Materials Today Sustainability 26:100752.

Hoai, P.T.T., T. Dai Lam, N.T.M. Huong and M.T. Van Anh. 2023. Removal of ethylene by synthesized Ag/TiO_2 photocatalyst under visible light irradiation. Chemosphere 329:138607.

Kashif, Z., M.Y. Naz, A. Maqbool, S. Shukrullah, M. Irfan, S.N. Faraj Mursal, S. Rahman and M.A. Magzoub Mohamed Ali. 2024. Study of dual Z-scheme photocatalytic response of TiO_2/Ag/ZnO coating on plasma-modified cotton fabric for self-cleaning application. AIP Advances 14:015222.

Kaur, D., K. Singh, W.T. Reynolds Jr and B. Pal. 2023. Graphene oxide-coated Ag-TiO_2 hybrid nanocomposites for superior photocatalytic activity. Environmental Science and Pollution Research 30:97660-97672.

Kudhier, M., R. Sabry, Y. Al-Haidarie and M. Al-Marjani. 2018. Significantly enhanced antibacterial activity of Ag-doped TiO_2 nanofibers synthesized by electrospinning. Materials Technology 33:220-226.

Kuruva, H., V.B. Khavala, B. Mishra, K. Murugan, T. Thomas and B. Murty. 2024. Solar-photocatalytic treatment of industrial wastewater using mechanically doped CNS-TiO_2 and synergistic TiO_2 incorporation: A promising cost-effective approach for industrial wastewater treatment. Materials Research Bulletin 177:112825.

Li, J., Y. Duan, L. Wang and J. Ma. 2024. Preparation of core-shell structure Ag@ TiO_2 plasma photocatalysts and reduction of Cr (VI): Size dependent and LSPR effect. Environmental Research 248:118265.

Mohammed, W., M. Matalkeh, R.M. Al Soubaihi, A. Elzatahry and K.M. Saoud. 2023. Visible light photocatalytic degradation of methylene blue dye and pharmaceutical wastes over ternary NiO/Ag/TiO_2 heterojunction. ACS omega 8:40063-40077.

Morante, N., V. Folliero, F. Dell'Annunziata, N. Capuano, A. Mancuso, K. Monzillo, M. Galdiero, D. Sannino and G. Franci. 2024. Characterization and Photocatalytic and Antibacterial Properties of Ag-and TiOx-Based (x= 2, 3) Composite Nanomaterials under UV Irradiation. Materials 17:2178.

Mustafa, Y.F. 2023. Modern developments in the application and function of metal/metal oxide nanocomposite–based antibacterial agents. BioNanoScience 13:840-852.

Narayan, J. and K. Bezborah. 2024. Recent advances in the functionalization, substitutional doping and applications of graphene/graphene composite nanomaterials. RSC advances. 14:13413-13444.

Nasseri, M.A., H. Keshtkar, M. Kazemnejadi and A. Allahresani. 2020. Phytochemical properties and antioxidant activity of Echinops persicus plant extract: Green synthesis of carbon quantum dots from the plant extract. SN Applied Sciences 2:1-12.

Nethravathi, P., G. Nagaraju and D. Suresh. 2022. TiO_2 and Ag-TiO_2 nanomaterials for enhanced photocatalytic and antioxidant activity: green synthesis using Cucumis melo juice. Materials Today: Proceedings 49:841-848.

Rahmawati, T., T. Butburee, W. Sangkhun, T. Wutikhun, J. Padchasri, P. Kidkhunthod, S. Phromma, T. Eksangsri, W. Kangwansupamonkon and P. Leeladee. 2023. Green synthesis of Ag-TiO_2 nanoparticles using turmeric extract and its enhanced photocatalytic activity under visible light. Colloids and Surfaces A: Physicochemical and Engineering Aspects 665:131206.

Saroha, J., E. Rani, M. Devi, P. Pathi, M. Kumar and S.N. Sharma. 2023. Plasmon-assisted photocatalysis of organic pollutants by Au/Ag-TiO_2 nanocomposites: a comparative study. Materials Today Sustainability 23:100466.

Shabaninia, M., M. Khorasani and S. Baniyaghoob. 2024. Synthesis of Silver-Doped Titanium Dioxide Nanoparticles by Sol-Gel and Coprecipitation Techniques: Evaluation of Antimicrobial Activity and Cytotoxic Effects. ChemistrySelect 9:1-22.

Shang, Y., Y. Chen and Z. Shi. 2013. Synthesis and visible light photocatalytic activities of Au/Cu_2O heterogeneous nanospheres. Acta Phys Chim Sin 29:1819-1826.

Sukhadeve, G., H. Bandewar, S. Janbandhu, J. Jayaramaiah and R. Gedam. 2023. Photocatalytic hydrogen production, dye degradation, and antimicrobial activity by Ag-Fe co-doped TiO_2 nanoparticles. Journal of Molecular Liquids 369:120948.

Tekin, D., T. Tekin and H. Kiziltas. 2020. Synthesis and characterization of TiO_2 and Ag/TiO_2 thin-film photocatalysts and their efficiency in the photocatalytic degradation kinetics of Orange G dyestuff. Desalination and Water Treatment 198:376-385.

Wu, H.-Y., W.-J. Jian, H.-F. Dang, X.-F. Zhao, L.-Z. Zhang and J.-H. Li. 2017. Hierarchical Ag-ZnO Microspheres with Enhanced Photocatalytic Degradation Activities. Polish Journal of Environmental Studies 26:871-880.

Zeng, Z., X. Tian, Y. Qian, Z. Wang, J. Liao, P. Li and X. Zhang. 2024. High Speed Shearing: A novel approach for high-quality ZnO nanoparticle synthesis and photocatalytic activity control. Powder Technology 433:119218.